Received: 18 July 2022 | Revised: 12 September 2022 | Accepted: 20 September 2022 | Published on: 13 October 2022

DOI: 10.1002/mrm.29482

RESEARCH ARTICLE

Magnetic Resonance in Medicine

Iterative training of robust k-space interpolation networks for improved image reconstruction with limited scan specific training samples

Peter Dawood[1] | **Felix Breuer**[2] | **Jannik Stebani**[2] | **Paul Burd**[3] | **István Homolya**[4] | **Johannes Oberberger**[5] | **Peter M. Jakob**[1] | **Martin Blaimer**[2]

[1]Department of Physics, University of Würzburg, Würzburg, Germany

[2]Magnetic Resonance and X-ray Imaging Department, Fraunhofer Institute for Integrated Circuits IIS, Division Development Center X-Ray Technology, Würzburg, Germany

[3]Institute for Theoretical Physics and Astrophysics, University of Würzburg, Würzburg, Germany

[4]Brain Imaging Centre, Research Centre for Natural Sciences, Budapest, Hungary

[5]Department of Internal Medicine I, University Hospital Würzburg, Würzburg, Germany

Correspondence
Peter Dawood, Department of Physics, University of Würzburg, Experimental Physics 5, Am Hubland, 97074, Würzburg, Germany.
Email: peter.dawood@physik.uni-wuerzburg.de

Funding information
Federal Ministry of Education and Research (BMBF), Grant/Award Number: 03VP04951; Bavarian Ministry of Economic Affairs, Infrastructure, Transport and Technology

Purpose: To evaluate an iterative learning approach for enhanced performance of robust artificial-neural-networks for k-space interpolation (RAKI), when only a limited amount of training data (auto-calibration signals [ACS]) are available for accelerated standard 2D imaging.

Methods: In a first step, the RAKI model was tailored for the case of limited training data amount. In the iterative learning approach (termed iterative RAKI [iRAKI]), the tailored RAKI model is initially trained using original and augmented ACS obtained from a linear parallel imaging reconstruction. Subsequently, the RAKI convolution filters are refined iteratively using original and augmented ACS extracted from the previous RAKI reconstruction. Evaluation was carried out on 200 retrospectively undersampled in vivo datasets from the fastMRI neuro database with different contrast settings.

Results: For limited training data (18 and 22 ACS lines for $R = 4$ and $R = 5$, respectively), iRAKI outperforms standard RAKI by reducing residual artifacts and yields better noise suppression when compared to standard parallel imaging, underlined by quantitative reconstruction quality metrics. Additionally, iRAKI shows better performance than both GRAPPA and standard RAKI in case of pre-scan calibration with varying contrast between training- and undersampled data.

Conclusion: RAKI benefits from the iterative learning approach, which preserves the noise suppression feature, but requires less original training data for the accurate reconstruction of standard 2D images thereby improving net acceleration.

KEYWORDS
complex-valued machine learning, data augmentation, deep learning, GRAPPA, parallel imaging, RAKI

1 | INTRODUCTION

Since its invention, MRI has become one of the most widespread clinical diagnostic techniques nowadays. It offers numerous benefits such as the absence of ionizing radiation, non-invasiveness, and the capability of showing soft tissue structures. However, MRI acquisitions can be time consuming and the total scanning time remains a crucial factor. Almost all MRI applications such as dynamic MR angiography, perfusion MRI, or imaging of the cardiac function require accelerated imaging to cover their typical time scales. Strategies to shorten the scan times based on hardware modifications have reached engineering as well as physiological limits (e.g., because of peripheral nerve stimulations). To further decrease scan time, data acquisition techniques based on gradient sub-encoding were considered. Parallel imaging (PI) is nowadays the most common acceleration strategy in clinical routine. In PI, the MR signal is acquired simultaneously with multiple, independent receiver coils (so-called phased arrays[1]), whereas the inverse image space (also known as k-space) is sub-sampled. Dedicated PI reconstruction methods make use of the inherent spatial encoding capabilities of the phased array to recover the full image content. They can be classified to operate either in image- or k-space domain. Image domain methods are essentially based on sensitivity encoding (SENSE)[2] and recover artifact-free images by using explicit spatial coil-sensitivity information. GRAPPA[3] is a widely used method operating in k-space and estimates missing k-space signals by a convolution of adjacent multichannel k-space signals. The convolution filters (also known as GRAPPA kernel) are calibrated by linear least-squares fit using several fully sampled auto-calibration signals (ACS) that serve as scan-specific training data. However, the matrix systems in PI typically suffer from ill-conditioning at high acceleration factors as the coil sensitivity encoding power is limited. The ill-conditioning produces severe noise enhancement in the reconstructed images, and is therefore a major limitation of traditional PI.

To improve the noise resilience, GRAPPA has been generalized recently within the machine learning framework by the deep learning method robust artificial-neural-networks for k-space interpolation (RAKI).[4] In contrast to GRAPPA, where only one convolution filter layer is applied for k-space interpolation, RAKI exploits multi-layer feature extraction. In RAKI, non-linearity is introduced by applying a non-linear activation function element-wise to the convolution-layers. The combination of multiple convolution layers with non-linear activation functions are essential elements of a convolutional neural network (CNN). Similar to GRAPPA, the neural network parameters in RAKI (i.e., the convolution filter weights within the CNN) are calibrated using scan-specific ACS as training data. In previous studies, RAKI has demonstrated better performance in comparison to GRAPPA.[4–6]

However, RAKI requires more training data because of its increased parameter space, which limits its applicability in standard 2D imaging, because the effective acceleration is significantly decreased. For small matrix sizes and high acceleration factors, the acquisition of the training data may take as long as the acquisition of the undersampled imaging data.

In the field of machine learning, a common way to deal with limited training data includes augmentation strategies.[7,8] For example, images can be rotated, flipped, or resized to generate additional training samples. However, applying these augmentation strategies in a straightforward manner does not work for multi-channel k-space interpolation methods such as RAKI (this is elaborated in more detail in the Methods section). The goal of k-space interpolation methods is to find an optimal combination (i.e., convolution filters) of measured k-space samples to reconstruct a missing sample. This combination strongly depends on the specific scan-setup including coil geometry, slice orientation, and phase-encoding direction.[9,10] For example, the optimal convolution filters are expected to differ between two neighboring imaging slices or between different breathing states as the coil sensitivities have different profiles. Hence, RAKI is often referred to as a scan-specific machine learning approach that does not depend on large databases for training.

This is contrary to many deep-learning parallel imaging reconstructions operating in image-space. They are often related to traditional supervised machine learning and generally rely on CNNs, which can be used to define generalized regularizers. This allows for higher computational complexity compared to regularizers that are used in classical compressed sensing,[11] such as image gradient or Tikhonov. The supervised learning process requires a set of fully sampled raw k-space data, acquired in a phased-array coil setup. The data is retrospectively undersampled and forms the input of the reconstruction network. The fully sampled data serves as the target reference image.[12] Therefore, the reconstruction parameters are learned from a large number of raw datasets.

Although RAKI does not require large databases for training, it cannot benefit from existing training data augmentation techniques. Therefore, alternative augmentation approaches have to be developed for RAKI.

In this work, we address the issue of limited training samples in RAKI by proposing an iterative training process, termed iterative RAKI (iRAKI). We demonstrate the flexibility of iRAKI for several 2D imaging and reconstruction scenarios with different contrast settings,

different calibration approaches (e.g., with pre-scan or integrated ACS) and implementation of phase-constrained reconstruction. Part of this work has been presented at the annual meeting of the ISMRM 2022.[13]

2 | METHODS

2.1 | Review of RAKI

RAKI can be seen as a generalization of GRAPPA, because it applies a multi-layer CNN instead of a single-layer convolution. In RAKI, the CNN parameters are trained on ACS and applied to acquired k-space signals for interpolating missing signals. The interpolation function to obtain signals of the nth set of evenly spaced missing lines of coil j can be expressed by,[4,12]

$$s_j\left(k_x, k_y - n\,\Delta k_y\right) = g_{j,c}\left(\left\{s_c\left(k_x - b_x\,\Delta k_x, k_y - R\,b_y\,\Delta k_y\right)\right\}_{b_x\in[-B_x,B_x],b_y\in[-B_y,B_y],c\in[1,N_c]}\right), \quad (1)$$

where $g_{j,c}$ stands for the layer-wise convolution of signals with non-linear activation in the receptive field of the CNN, R denotes the undersampling rate and N_C denotes the coil number. The extent of the receptive field is specified by the parameters B_x and B_y in readout and phase-encoding direction, respectively. The parameters B_x and B_y are effective convolution filter sizes and depend on the filter sizes of each single layer. A detailed description of Equation (1) for this work is given in the following section.

2.2 | Tailored RAKI network

In this work, RAKI was tailored for improved performance with limited amount of training data. The network architecture used in this work is depicted in Figure **S1A**. We implemented a single CNN for simultaneous multi-coil k-space interpolation, rather than assigning each single coil one CNN as implemented in original RAKI. In this way, the correlations and interactions between all coils are preserved. Furthermore, instead of performing real-valued convolution, we implemented its complex-valued equivalent.[14,15] As nonlinear activation function, we used the leaky variant of the complex rectifier linear unit (ℂReLU)[15,16]:

$$\mathbb{C}\text{LeakyReLU}(\boldsymbol{z}) = \text{LeakyReLU}(\text{Re}\{\boldsymbol{z}\}) + i\ \text{LeakyReLU}(\text{Im}\{\boldsymbol{z}\}), \quad (2)$$

with $\text{Re}\{\mathbf{z}\}$ and $\text{Im}\{\mathbf{z}\}$ denoting the real and imaginary part of signal $\boldsymbol{z}$, respectively, i denoting the imaginary unit, and LeakyReLU is the leaky variant of the standard real-valued rectifier linear unit.[17] Note, that the total number of hidden layers, the assigned channel-number for each layer, the learning rate as well as the slope for ℂLeakyReLU were determined heuristically in a hyperparameter search, because currently there are no existing methods for optimally tuning the network-architecture in deep learning applications.[18,4] Especially the convolution kernel sizes were tailored for the case of a limited training data amount. The hyperparameter optimization resulted in the following network architecture: The input layer s_1 takes the complex-valued, zero-filled multi-coil k-space data, resulting in N_c total input channels, with N_c being the number of receiver coils. The hidden layers s_2 and s_3 are then calculated through linear, complex-valued convolution, and an element-wise activation using a leaky complex rectifier linear unit ℂLeakyReLU: $\boldsymbol{s_2} = \mathbb{C}Leaky\ \text{ReLU}(\boldsymbol{s_1} \circledast \boldsymbol{W_C^1})$ and $\boldsymbol{s_3} = \mathbb{C}\text{Leaky ReLU}(\boldsymbol{s_2} \circledast \boldsymbol{W_C^2})$, with the complex convolution matrix $\boldsymbol{W_C^1}$ of size $k_y \times k_x = 2 \times 5$ and $\boldsymbol{W_C^2}$ of size $k_y \times k_x = 1 \times 1$ in phase-encoding and readout direction, respectively. The first hidden layer $\boldsymbol{s_2}$ is assigned 256 channels and the second hidden layer $\boldsymbol{s_3}$ is assigned 128 channels. The output layer $\boldsymbol{s_4}$ predicts all missing points across all coils simultaneously, therefore having $(R-1) \times N_c$ channels, where R denotes the undersampling rate. It is activated with the identity function $\gamma(x) = x$, therefore, reading $\boldsymbol{s_4} = \gamma(\boldsymbol{s_3} \circledast \boldsymbol{W_C^3})$, with $\boldsymbol{W_C^3}$ of size $k_y \times k_x = 1 \times 5$. The mean-squared-error (MSE) of signal prediction $\boldsymbol{y}$ to its groundtruth $\hat{\boldsymbol{y}}$ was used as cost function $L(\boldsymbol{y}, \hat{\boldsymbol{y}})$ for training,

$$L(\boldsymbol{y}, \hat{\boldsymbol{y}}) = \frac{1}{N}\left(\sum_{i=0}^{N} |\boldsymbol{y_i} - \hat{\boldsymbol{y}}_i|^2\right), \quad (3)$$

with N denoting the total number of training samples. The adaptive moment estimation (Adam) optimizer[19] was chosen as optimization algorithm to minimize the mean-squared-error of estimated k-space data to its ground-truth. Bias terms were excluded in the CNN, because they may perturb k-space scaling.[4] The CNN was implemented within the PyTorch package 1.8.0.[20] To obtain the final reconstructed image, the interpolated k-spaces are Fourier-transformed and combined by root sum-of-squares.

We compared our tailored RAKI implementation against the publically available original implementation on 200 datasets assembled from the fastMRI neuro database[21] (see section "2.4.1 Datasets" for details). The datasets were fourfold retrospectively undersampled, and 22 ACS lines were used for evaluation.

Note that the GRAPPA k-space reconstruction via convolution can be formulated as $\boldsymbol{s_{int}} = \gamma\left(\boldsymbol{s_1} \circledast \boldsymbol{W_C^G}\right)$, where $\boldsymbol{s_{int}}$ denotes the interpolated k-space signals, $\boldsymbol{s_1}$ denotes the undersampled, multi-coil k-space data, $\boldsymbol{W_C^G}$ is the

GRAPPA kernel, and γ is the identity function assigned to the only convolution layer. Therefore, the model in GRAPPA can be obtained from the RAKI model by omitting the hidden layers, which are used for abstract multi-layer feature extraction of k-space signals. Therefore, essentially, GRAPPA can be seen as a reduced version of RAKI.[4] All reconstructions were performed on a high-performance-computing-cluster with Intel Xeon Gold 6134 (CPU).

2.3 | Iterative training

Because k-space interpolation is based on correlations between adjacent points and redundancies induced by coil sensitivity profiles, the effective convolution filter size determines the extent in which the k-space footprint of spatially varying coil sensitivity profiles is captured.

Previous works have shown that a larger kernel size in general is beneficial for k-space interpolation as it yields improved image reconstruction.[22] However, the use of a larger kernel requires more ACS. The common strategy to handle the issue of limited training data is to use data augmentation techniques to synthetically enlarge the effective amount of training data. Sandino et al.[23] trained unrolled neural networks on augmented 2D cardiac cine MRI data in image space (e.g., by random flipping along readout- and phase-encoding direction) or random circular translations along phase-encoding direction. However, these augmentation techniques do not work for k-space interpolation in standard 2D imaging, because the multi-channel k-space correlations must be preserved. The phase-encoding direction must be coherent with the underlying coil geometry for estimation of convolution filters. However, an image rotation, −stretching or –compression comes along with corresponding operations on the coil geometry. Therefore, the coherence of the convolution filter and k-space points is lost, as the underlying basis functions to be combined change as well. Therefore, one cannot find the searched filter parameters with the augmented data for standard Cartesian undersampling.

For the case of simultaneous multi-slice (SMS) imaging, Nencka et al.[24] demonstrated an augmentation strategy for specialized RAKI networks. In SMS, additional acceleration is achieved by the simultaneous excitation of multiple slices via dedicated RF-pulses. To separate the aliased slices, RAKI has to be adapted to this specific reconstruction problem. To improve the separation of aliased slices, Nencka et al. generated additional synthetic k-space signals via linear combination of k-space observations for subsets of the target slices in the excited package. For standard 2D imaging, however, this approach is not applicable because of the lack of multiple slice excitations.

As illustrated in Figure 1, the proposed iterative training in iRAKI includes different amounts of original and augmented ACS, as well as different convolution filter sizes. The goal is to enhance RAKI image quality when only a reduced amount of original acquired ACS is available. The training in iRAKI is a three step procedure. In a first step, an initial GRAPPA reconstruction is performed using 18 and 22 original ACS lines for $R = 4$ and $R = 5$, respectively, to obtain augmented ACS (including re-inserted original ACS). In this work, GRAPPA is assigned a kernel size 2×5 and Tikhonov regularization is applied (singular values less than or equal to $\lambda * \sigma_{max}$ are set to zero, with σ_{max} denoting the largest singular value of the calibration matrix, and $\lambda = 1e{-}4$). In the second step, $N = 65$ central lines of the initial GRAPPA k-space reconstruction (including both re-inserted original and augmented ACS) are used to train RAKI initially. The first hidden layer in RAKI is assigned a filter size 4×7 in phase-encoding (PE)- and readout (RO)-direction, respectively. Inspired by iterative-GRAPPA[25], subsequent iteration steps follow to refine the CNN weights in the third step. In each iteration, the CNN weights are transferred, and further optimized using $N' = 65$ central lines (including both re-inserted original and augmented ACS) from the RAKI reconstruction of the previous iteration. The initial learning rate η_0 passed to the Adam optimizer is decreased by a constant factor $\Delta\eta$ after each subsequent iteration step. Therefore, the learning rate at iteration step number j reads $\eta_j = \eta_0 - j \cdot \Delta\eta$. In this work, we set empirically $\eta_0 = 5e-3$ and $\Delta\eta = 2e-4$ for $R = 4$, and $\Delta\eta = 3e-4$ for $R = 5$. We chose $\Delta\eta$ heuristically such that the cost function (MSE) does not diverge at late iteration steps, ensuring robustness in the iterative training procedure. Accordingly, the total number of iterations N_{iter} amounts to $N_{iter} = \eta_0/\Delta\eta$. The final optimized CNN interpolates the multi-coil sub-sampled k-spaces simultaneously, which are then Fourier-transformed to image domain, and combined via root sum-of-squares coil combination to obtain the final reconstructed image.

2.4 | Experiments

2.4.1 | Datasets

To study the performance of iRAKI across a larger cohort, it was tested on 10 fully sampled datasets randomly selected from the fastMRI[21] neuro-database, with the first five slices reconstructed in each case. Four different contrasts (T_1, T_1post, T_2, and fluid attenuated inversion recovery [FLAIR]) were considered, resulting in a total of 200

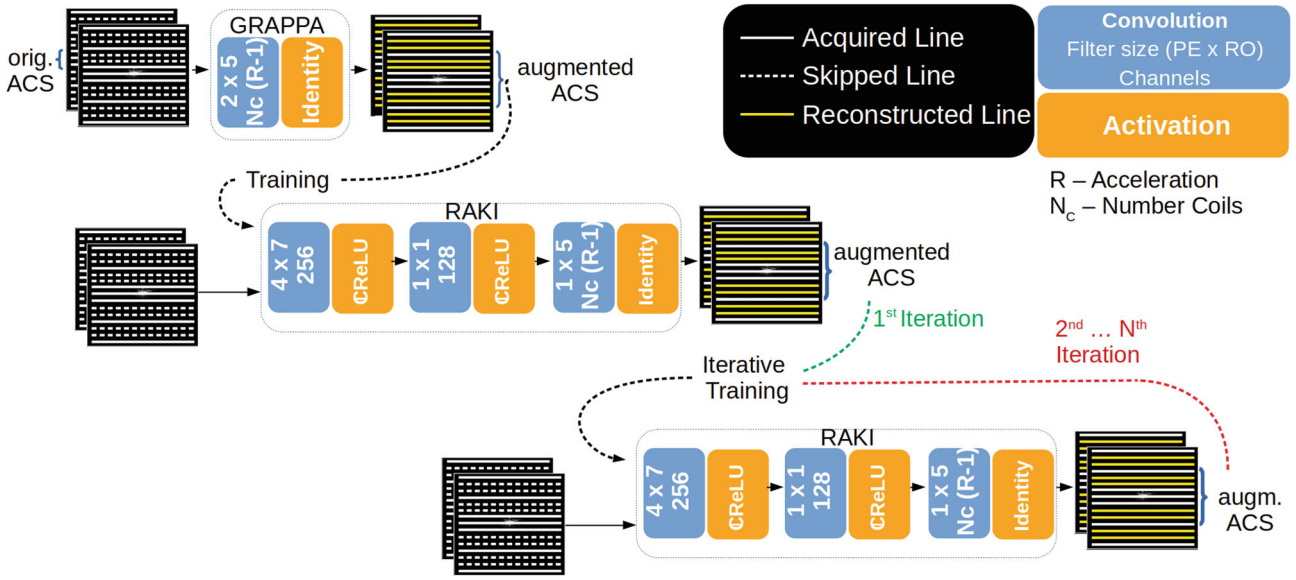

FIGURE 1 Workflow of iRAKI. RAKI is initially trained with augmented ACS obtained from an initial GRAPPA reconstruction using a kernel size 2 × 5 (phase- × readout-direction). The first hidden layer in RAKI is assigned a convolution filter size 4 × 7. From the initial GRAPPA reconstruction, $N = 65$ central k-space lines are used as training samples for RAKI training. In subsequent iteration steps, the CNN weights are further optimized using $N' = 65$ central lines from the RAKI reconstruction of the previous iteration step as ACS. Original ACS are inserted after each reconstruction step. The learning rate is decreased by a constant factor after each iteration step, which determines the total iteration number, given an initial learning rate. iRAKI, iterative robust artificial-neural-networks for k-space interpolation; ACS, auto-calibration signals

slices for evaluation. For training, 18 and 22 original ACS lines were used for four- and fivefold retrospective undersampling, respectively.

Additionally, three in-plane brain imaging datasets were acquired on healthy volunteers at 3T (Siemens Magnetom Skyra, Siemens Healthineers) using a 20-channel head–neck coil array, with only 16 coils activated. The study was approved by our institutional review board. Written informed consent was obtained before each in vivo study.

One dataset is referred to as neuro1, acquired using FLASH with T_1-weighting (TR-/TE: 250/2.9 ms, flip angle: 70°, FOV: 230 × 230 mm^2, matrix-size: 320 × 320, slice-thickness: 3.0 mm).

Furthermore, a T_1- and T_2-weighted neuro imaging was carried out subsequently (referred to as neuro2) using Turbo-Spin-Echo with the following imaging parameters for T_1-weighting: TR-/TE: 500/10.0 ms, flip angle: 90/180°, FOV: 193 × 220 mm^2, matrix-size: 224 × 256, slice-thickness: 4.0 mm. The T_2-weighting imaging parameters read: TR-/TE: 4500/102.0 ms, flip angle: 90/180°, FOV: 193 × 220 mm^2, matrix-size: 230 × 256, slice-thickness: 4.0 mm

This experiment was carried out on another subject (neuro3) using Turbo-Spin-Echo with a fat saturation module for the T_1-weighted image with following imaging parameters: TR-/TE: 600/6.4 ms, flip angle: 90/180, FOV: 199 × 220 mm^2, matrix-size: 320 × 320, slice-thickness: 4.0 mm. The T_2-imaging parameters read: TR-/TE: 4500/95 ms, flip angle: 90/180, FOV: 200 × 220 mm^2, matrix-size: 320 × 320, slice-thickness: 4.0 mm.

A fourth dataset (referred to as neuro4) was acquired using FLASH with T_1-weighting (TR/TE: 250/3.1 ms, flip angle: 70, FOV: 195 × 250 mm^2, matrix-size: 250 × 320, slice-thickness: 4.0 mm). This scan was prospectively undersampled at rate 4. A pre-scan with PD-weighting (matrix size: 64 × 64) was acquired beforehand to study the performance of iRAKI in case of strongly varying contrast information (see section "2.4.3 Pre-scan calibration" below).

2.4.2 | In-line calibration

All datasets were retrospectively undersampled, and 18 and 22 ACS lines were used as training data for four- and fivefold uniform undersampling, respectively. Original ACS were re-inserted into the final reconstructed k-space. To provide comparable results to image-based deep-learning approaches, both the reference and the reconstructed image were masked to compute numeric metrics such as normalized mean squared error (NMSE), structural-similarity-index-measure (SSIM)[26] and peak-signal-to-noise-ratio (PSNR). The masks were

derived from the standard coil mapping procedure with ESPIRiT.[27] In addition, all image reconstructions were evaluated qualitatively via error images.

The model complexity of the CNN in RAKI is significantly determined by its convolution filter sizes. Analogous to GRAPPA, the choice of the filter sizes affects the total number of available training data, given a fixed number of ACS lines.[22] As both complexity and total number of training data are crucial factors for the performance of the CNN, a more detailed evaluation for this trade-off is obligatory. For this purpose, we vary the number of ACS lines between $N_{ACS} = 15, \ldots, 100$ with step size 5, and assign two different convolution filter sizes to the first convolution filter in the CNN (denoted as $\boldsymbol{W}_C^1$ in section 2.2): $k_y \times k_x = 2 \times 5$ and 4×7, respectively. Image reconstruction quality is assessed qualitatively via error images and quantitatively via the NMSE of the magnitude image with respect to (w.r.t.) the fully sampled reference image. For comparison, the NMSE of the corresponding GRAPPA reconstruction is evaluated. In all cases, to investigate the reconstruction performance only, ACS were not re-inserted into the final reconstructed k-space.

2.4.3 | Pre-scan calibration

In the in-line calibration acquisition scheme, the scan-specific training data used to calibrate the GRAPPA kernel and the model weights in iRAKI can be re-inserted into the reconstructed k-spaces, because the ACS are an integral part of the image scan. Alternatively, the training data can be obtained by acquiring a fully sampled, low resolution pre-scan before the actual undersampled image scan series. Because no contrast information is needed in the standard parallel imaging, the pre-scan sequence parameters like TR- and TE can be adjusted to maximize SNR, or to minimize the total acquisition time. The pre-scan approach is also useful for the acquisition of an image series with high temporal resolution, or in combination with sequences that require uniform undersampling (e.g., Echo-Planar-Imaging). However, for these cases, the training data cannot be re-inserted into to the reconstructed k-space of the actual image scan. Therefore, the performance of iRAKI needs to be investigated separately for pre-scan ACS with different contrast. For this purpose, we acquired a proton-density weighted pre-scan of size 64×64 in PE-and RO-direction, which was used to calibrate GRAPPA, RAKI, and iRAKI. The training procedure in iRAKI with pre-scan calibration setting differs from in-line calibration setting described in section 2.3 "Iterative training" only by omitting the re-insertion of the original training data back into reconstructed k-spaces. Please note that the pre-scan provides 64 ACS lines. However, the number of readout points is also reduced to 64 (compared to, e.g., 320 readout points in the imaging scans). The calibrated models were then used to reconstruct a subsequently acquired, fourfold prospectively undersampled 2D neuro image scan with T_1-weighting (referred to as neuro4).

2.4.4 | Phase-constrained reconstruction

The virtual conjugate coils (VCC) concept[28] has been introduced to improve parallel MRI performance by using conjugate symmetry properties of the k-space, and can be seen as a phase-constrained reconstruction technique. From actual physical coils, additional virtual coils are generated, which contain conjugate symmetric k-space signals. Thereby, additional image phase and coil phase information is used to improve reconstruction conditions. The VCC concept has been presented as a practical approach especially in combination with GRAPPA, because no explicit spatial phase information is required. In this work, we study the influence of VCCs on the reconstruction quality of RAKI and iRAKI in comparison to GRAPPA. The additional k-space signals from a virtual coil can be generated from an actual coil h according to,

$$\boldsymbol{s}_{h+N_c}(\boldsymbol{k}) = \boldsymbol{s}_h^*(-\boldsymbol{k}),\ h = 1 \ldots N_c, \tag{4}$$

where N_c denotes the number of actual physical coils in the phased array, $\boldsymbol{k}$ denotes a k-space vector and $\boldsymbol{s}_h^*$ is the complex conjugate signal assigned to coil h. The stack of virtually received k-spaces therefore contains two times as many coils as actual coils. The reconstruction process is carried out by first generating the virtual coils for both ACS and undersampled data according to Equation (4), and subsequently performing a k-space reconstruction using a standard GRAPPA-, RAKI- or iRAKI reconstruction. The resulting images of the physical coils are then combined using a root sum-of-squares combination.

2.4.5 | Comparison to end-to-end variational network

We compared the performance of iRAKI to an image-based variational network (VarNet)[29] for two scenarios:

- Single anatomy: VarNet training on knee datasets, image reconstruction of undersampled knee datasets with matching contrast.
- Cross-anatomy: VarNet training on knee datasets, image reconstruction of undersampled neuro datasets with different contrast (i.e. scans from the fastMRI cohorts).

We used a VarNet from BART[30] that was pre-trained on 20 uniformly undersampled ($R = 4$) knee datasets (10 slices each) with proton-density weighting. The training data was assembled from knee datasets of proton-density weighting of the original VarNet publication.[29] Coil sensitivity maps were computed with ESPiRIT[27] using 27 ACS lines. The same undersampled datasets were reconstructed with iRAKI using 27 original ACS lines for training.

3 | RESULTS

3.1 | Network tailoring

The tailored RAKI model was compared to the original RAKI implementation on a total of 200 datasets assembled from the fastMRI neuro database. At fourfold retrospectively undersampling and 22 ACS lines as training data, our tailored variant achieved NMSE-medians reduced by 33.51%, 43.21%, 34.53%, and 27.98% for T_1, T_1post, T_2, and FLAIR-weighting, respectively (Figure **S1B**). On a visual scale, the tailored network strongly suppresses residual artifacts compared to the original implementation (Figure **S1C**). Based on these results, we consider the tailored variant as the favored model for this manuscript, and all subsequently shown RAKI-reconstructions were obtained from the tailored RAKI implementation described in the section "2.1. Review of RAKI" and denoted as standard RAKI.

3.2 | Experiments

3.2.1 | Training data amount

Figure 2 depicts the NMSE of GRAPPA, RAKI, and iRAKI at fourfold retrospectively undersampling of the neuro1 dataset in dependence of the number of ACS lines in range 15 to 100. Both GRAPPA and RAKI were evaluated with two different kernel sizes (2×5 and 4×7 in PE $\times$ RO direction). Although standard RAKI deteriorates rapidly for ACS amounts <20 lines at both kernel sizes, we notice that iRAKI is much more robust in the limit of only a few ACS lines (note that training data is not re-inserted). For ACS amounts exceeding 50 lines, the larger kernel size in standard RAKI outperforms the smaller kernel size, which is the reason why the former is favored in iRAKI. On a visual scale (Figure 3), we notice that iRAKI trained with 15 original ACS lines yields a reconstruction quality that is comparable to standard RAKI trained with 100 original ACS lines (also shown by numeric results from top to bottom: NMSE, PSNR, and SSIM). For all configurations

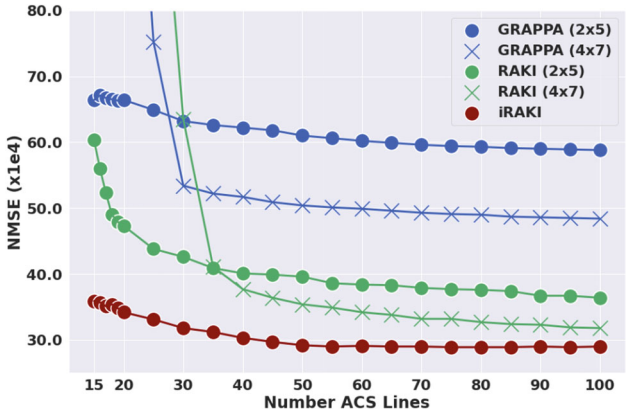

FIGURE 2 The NMSE of GRAPPA, standard RAKI and iRAKI in dependence of the number of ACS lines used as training data for fourfold undersampled neuro1 dataset. GRAPPA and standard RAKI were evaluated for two kernel sizes assigned to the first convolution layer (2×5 and 4×7 in phase-encoding $\times$ readout direction). ACS were not re-inserted into reconstructed k-spaces. Corresponding image reconstructions are included in Supporting Material S1. NMSE, normalized mean-squared-error; RAKI, robust artificial-neural-networks for k-space interpolation; iRAKI, iterative RAKI; ACS, auto-calibration signals

evaluated in Figure 2, corresponding image reconstructions with error maps and quantitative metrics have been compiled in a movie, which can be found in Supporting Material S1. The movie underlines that residual artifacts, which appear in standard RAKI at low ACS amounts (<25 lines) are being gradually suppressed with successively increasing ACS amount.

3.2.2 | In-line calibration

Figure 4 shows boxplots of the NMSE and SSIM metrics for GRAPPA, RAKI, and iRAKI evaluated on fastMRI cohorts with T_1, T_1post, T_2, and FLAIR contrasts. Although GRAPPA is generally outperformed for both $R = 4$ and $R = 5$, iRAKI enhances standard RAKI as it yields NMSE medians systematically reduced by 26.4%, 28.7%, 26.2%, and 21.7% for T_1, T_1post, T_2, and FLAIR, respectively, for $R = 4$ and 28.3%, 36.4%, 32.6%, and 30.4% for $R = 5$. The SSIM medians are systematically enhanced by 1.5%, 1.4%, 1.7%, 1.6% ($R = 4$) and 2.3%, 2.6%, 3.4%, 3.7% ($R = 5$) for T_1, T_1post, T_2, and FLAIR, respectively.

Figure 5 depicts exemplary GRAPPA, standard RAKI and iRAKI image reconstructions for all evaluated contrasts from the fastMRI cohorts at fourfold retrospectively undersampling and 18 ACS lines (see Figure 6 for fivefold retrospectively undersampling and 22 ACS lines). We note that GRAPPA, as expected, suffers from pronounced noise enhancement. Standard RAKI provides noise-resilience,

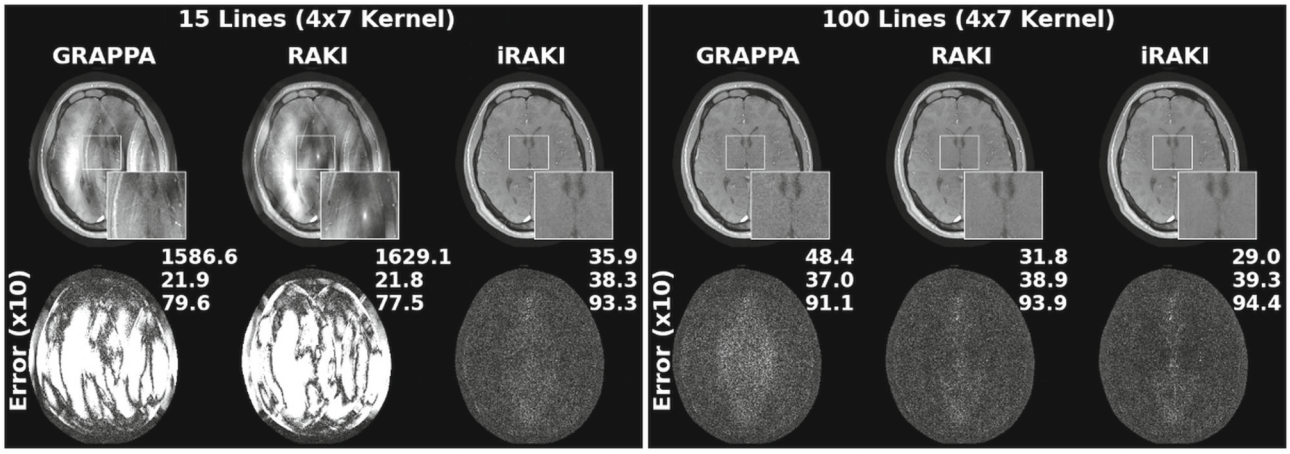

FIGURE 3 GRAPPA, standard RAKI and iRAKI in comparison at 15 and 100 ACS lines as training data (left- and right-hand side, respectively) using a convolution kernel of size 4×7 (phase- $\times$ readout-direction) assigned to the first convolution layers. Note that the depicted images correspond to samples shown in Figure 2. Error maps with respect to the fully sampled reference image are shown at the bottom including NMSE, PSNR, and SSIM difference-metrics. RAKI, robust artificial-neural-networks for k-space interpolation; iRAKI, iterative RAKI; ACS, auto-calibration signals; NMSE, normalized mean-squared-error; PSNR, peak-signal-to-noise-ratio; SSIM, structural-similarity-index-measure

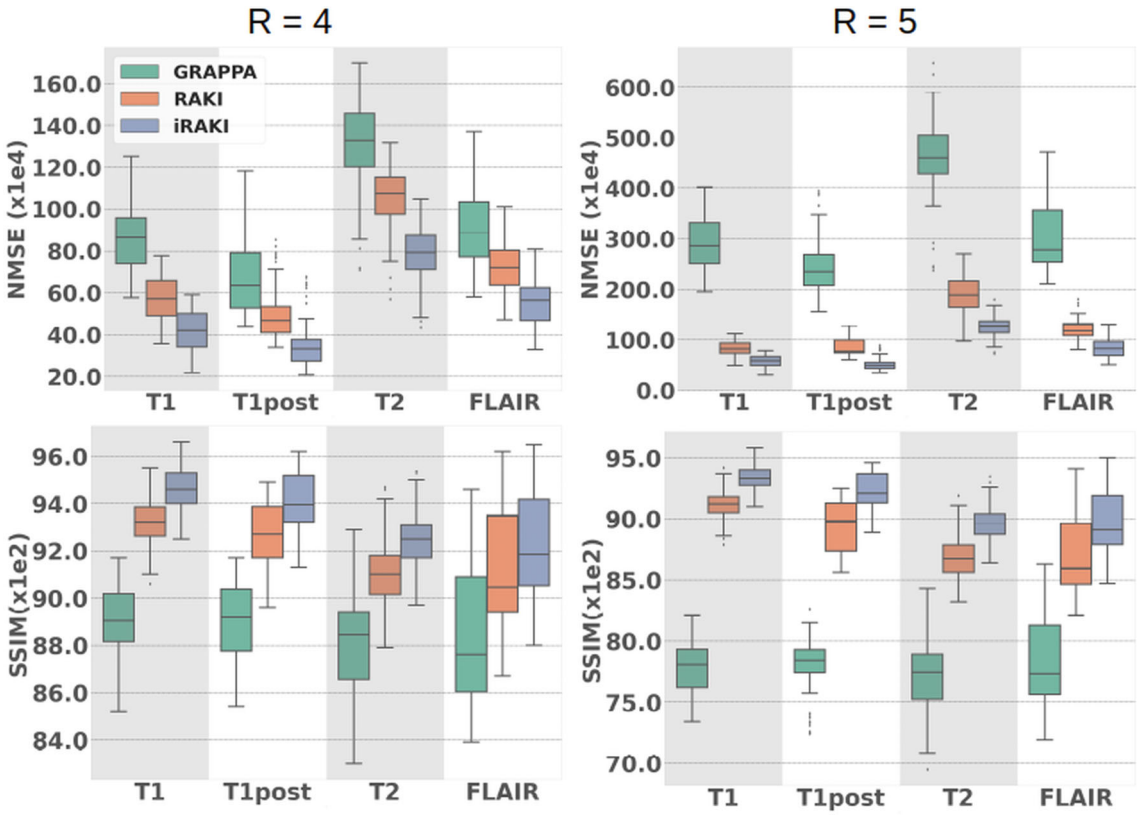

FIGURE 4 Boxplots of NMSE (top) and SSIM (bottom) for GRAPPA, standard RAKI and iRAKI evaluated on cohorts assembled from the fastMRI neuro database. Four different contrast were considered (T_1, T_1post, T_2 and FLAIR), and 50 datasets per contrast were retrospectively undersampled at rate 4 (left) and rate 5 (right) using 18 and 22 ACS lines, respectively. Exemplary image reconstructions are depicted in Figure 5 ($R = 4$) and Figure 6 ($R = 5$). NMSE, normalized mean-squared-error; SSIM, structural-similarity-index-measure; RAKI, robust artificial-neural-networks for k-space interpolation; iRAKI, iterative RAKI; FLAIR, fluid attenuated inversion recovery; ACS, auto-calibration signals

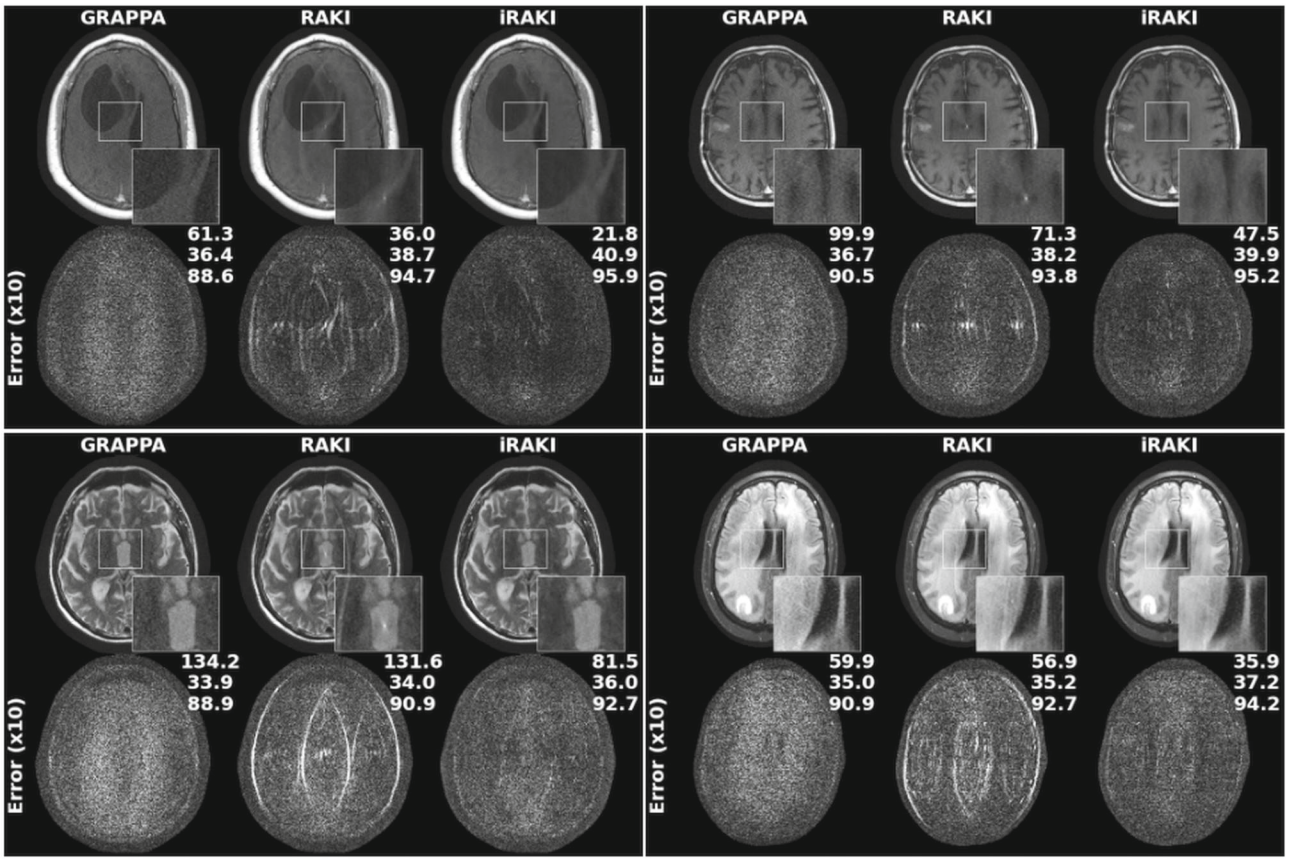

FIGURE 5 GRAPPA, standard RAKI and iRAKI reconstructions for exemplary sample datasets from evaluated fastMRI cohorts (see Figure 4, from left to right, and top to bottom: T_1, T_1post, T_2 and FLAIR). Error maps are shown at the bottom and include NMSE, PSNR, and SSIM w.r.t. the fully sampled reference image. Datasets were fourfold retrospectively undersampled, and 18 ACS lines were used as training data (re-inserted into reconstructed k-space). RAKI, robust artificial-neural-networks for k-space interpolation; iRAKI, iterative RAKI; FLAIR, fluid attenuated inversion recovery; NMSE, normalized mean-squared-error; PSNR, peak-signal-to-noise-ratio; SSIM, structural-similarity-index-measure; ACS, auto-calibration signals

however, suffers from residual artifacts because of limited training data amount for both acceleration factors. iRAKI, however, incorporates desirable features of both GRAPPA and standard RAKI by suppressing noise enhancement and residual artifacts, respectively, resulting in improved visual appearance and outperforming NMSE, PSNR, and SSIM for all depicted examples.

Similar outcomes are obtained from three acquired in-plane imaging experiments neuro1–3, for both T_1-and T_2-weighting and $R = 4$ and $R = 5$ (Figures S2–S6, respectively, for image reconstructions with error maps and numeric difference metrics).

3.2.3 | Pre-scan calibration

Figure 7 depicts results of GRAPPA, standard RAKI, and iRAKI using the pre-scan as training data to reconstruct the fourfold accelerated neuro4 dataset. Note that the contrast information in the pre-scan (proton-density) varies from that of the undersampled image scan (T_1). We observe that standard RAKI is deteriorated because of contrast-loss artifacts (contrast of ACS data sneaks into reconstruction); however, it yields less noise-amplification in comparison to GRAPPA, which maintains contrast. Moreover, iRAKI does not reveal "contrast-loss" artifacts appearing in standard RAKI, but preserves its improved noise resilience in comparison to GRAPPA, without the cost of blurring artifacts. We emphasize that iRAKI combines advantages of both GRAPPA and RAKI (more natural contrast and stronger noise suppression, respectively), therefore, providing an improved visual appearance.

3.2.4 | Phase-constrained reconstruction

Figure 8 depicts comparisons of iRAKI with iRAKI including phase constraints via the VCC concept (iRAKI-VCC) using the T_1-neuro1 and the T_2-neuro3 datasets. For both four- and fivefold undersampling using 18 and 22 original

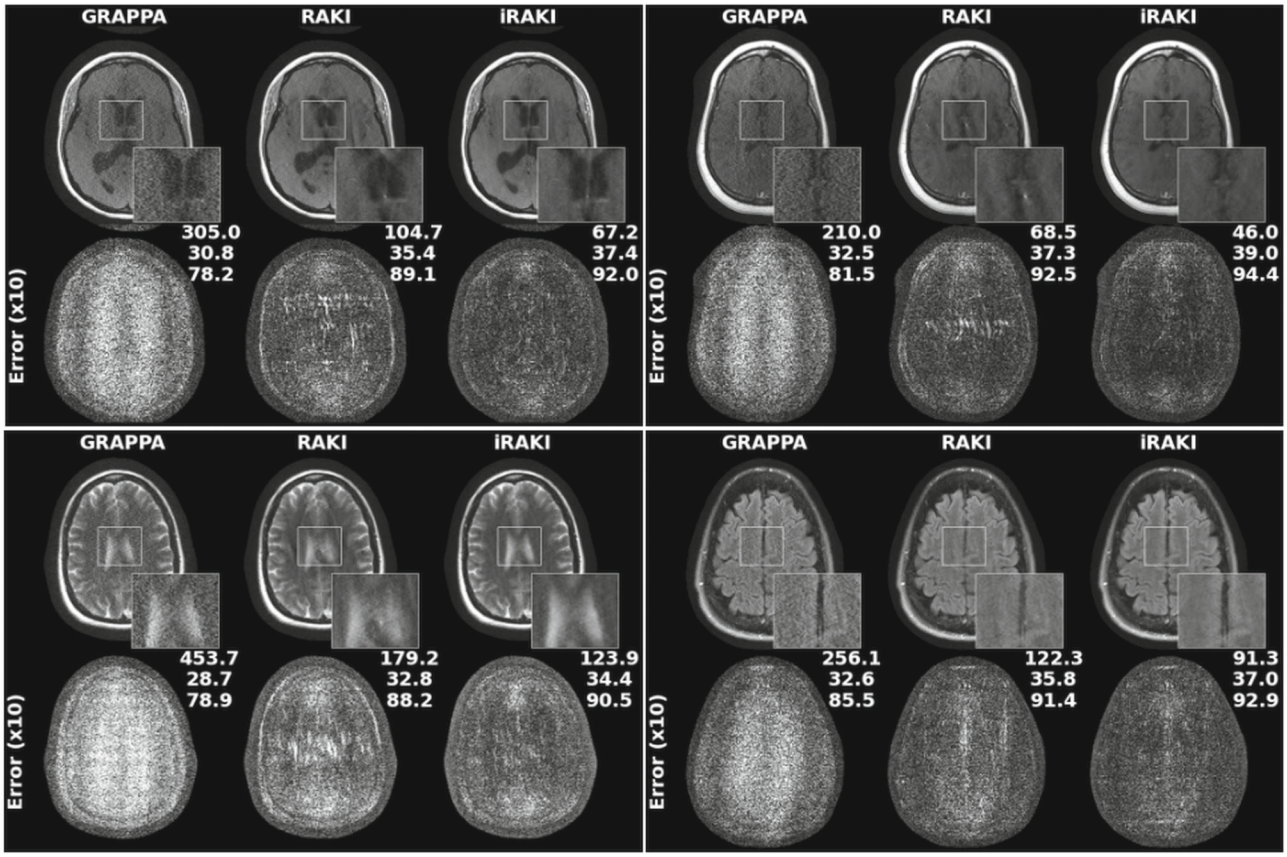

FIGURE 6 GRAPPA, standard RAKI and iRAKI reconstructions for exemplary sample datasets from evaluated fastMRI cohorts (see Figure 4, from left to right, and top to bottom: T_1, T_1post, T_2 and FLAIR). Error maps are shown at the bottom and include NMSE, PSNR, and SSIM w.r.t. the fully sampled reference image. Datasets were fivefold retrospectively undersampled, and 22 ACS lines were used as training data (re-inserted into reconstructed k-space). RAKI, robust artificial-neural-networks for k-space interpolation; iRAKI, iterative RAKI; FLAIR, fluid attenuated inversion recovery; ACS, auto-calibration signals

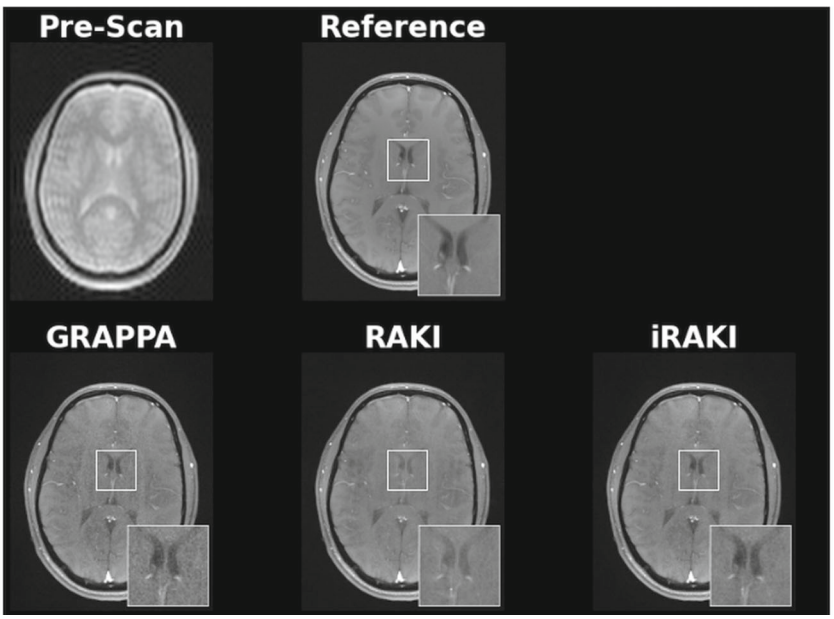

FIGURE 7 A pre-scan (top row) served as training data for image reconstructions of prospectively fourfold undersampled image scan (neuro4) via GRAPPA, standard RAKI and iRAKI (bottom row). Because of the different contrasts, the training data from the pre-scan was not re-inserted after image reconstructions. RAKI, robust artificial-neural-networks for k-space interpolation; iRAKI, iterative RAKI

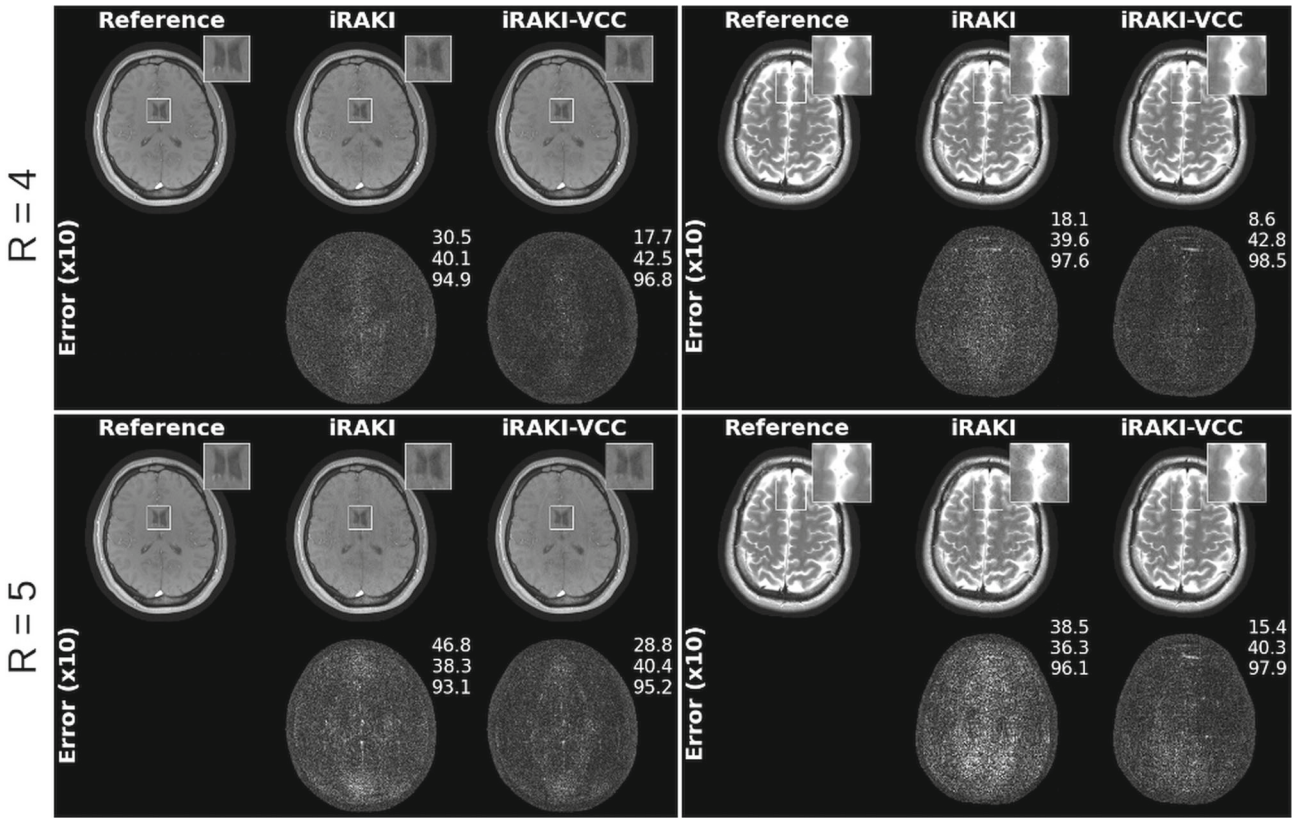

FIGURE 8 iRAKI in comparison to phase-constrained iRAKI via the VCC concept (iRAKI-VCC) at four- and fivefold retrospective undersampling (top and bottom row, respectively), evaluated on the T_1 neuro2- (left column) and T_2 neuro3 datasets (right column). Error maps are shown at the bottom and include NMSE, PSNR, and SSIM w.r.t. the fully sampled reference image. iRAKI, iterative robust artificial-neural-networks for k-space interpolation; VCC, virtual-conjugate-coils; NMSE, normalized mean-squared-error; PSNR, peak-signal-to-noise-ratio; SSIM, structural-similarity-index-measure

ACS lines, respectively, iRAKI-VCC enhances standard iRAKI as it yields improved suppression of both residual artifacts and noise-enhancement, leading to greatly improved visual appearance and improved NMSE, PSNR, and SSIM.

Note that comparisons of GRAPPA, standard RAKI, and iRAKI with and without VCC included for all three datasets neuro1-neuro3 are depicted in the Figures S2–S6, respectively. We underline that standard RAKI-VCC provides improved noise resilience in comparison to GRAPPA-VCC; however, it still reveals residual artifacts, which are not apparent in iRAKI-VCC.

3.2.5 | Comparison to image-based end-to-end variational network

Figure 9A depicts a fourfold retrospectively undersampled T_1 knee dataset reconstructed using iRAKI, and a variational network (VarNet). The VarNet was trained on a database of knee datasets with matching contrast. Although both iRAKI and the VarNet provide high quality reconstructions, the VarNet shows improved denoising effects, because it reveals a better noise resilience in comparison to iRAKI, also indicated by improved quantitative metrics.

However, using the same VarNet to reconstruct a fourfold retrospectively undersampled dataset from the T_1post fastMRI neuro database, which represents a cross-domain task regarding anatomy and contrast of the target image, we occasionally observe the emerge of severe residual artifacts, as exemplary depicted in Figure 9B. Moreover, iRAKI generally retains its improved reconstruction quality, and shows high flexibility across different anatomy- or contrast information. The above mentioned findings were also observed for datasets of the fastMRI cohorts with T_1-, T_2-, and FLAIR-weighting (see Figure S7 for exemplary image reconstructions).

4 | DISCUSSION

This study aimed to enhance the deep-learning method RAKI in the limit of only few ACS lines in standard 2D

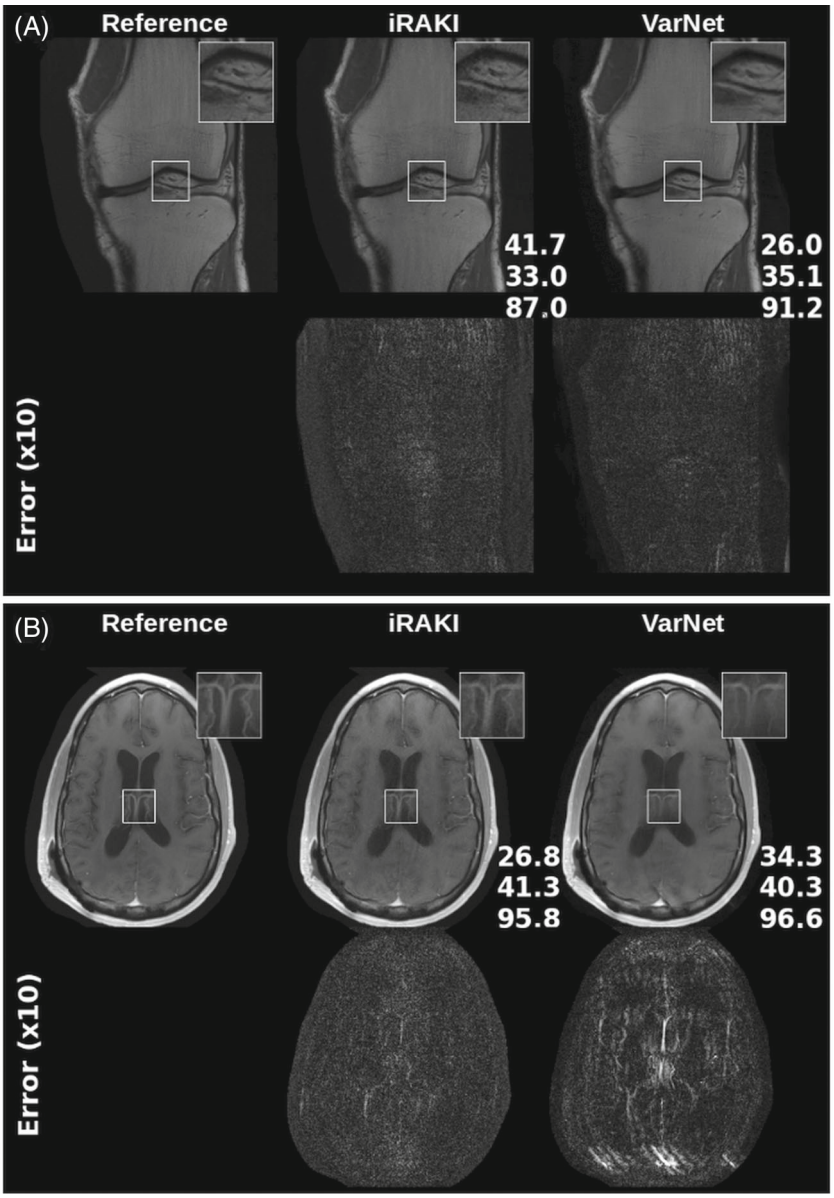

FIGURE 9 Comparison between iRAKI and VarNet (A) with matching anatomy and contrast in training- and reconstructed data and (B) with non-matching anatomy and contrast. Error maps are shown at the bottom and include NMSE, PSNR, and SSIM w.r.t. the fully sampled reference image. iRAKI, iterative robust artificial-neural-networks for k-space interpolation; VarNet, variational network; NMSE, normalized mean-squared-error; PSNR, peak-signal-to-noise-ratio; SSIM, structural-similarity-index-measure

imaging. To this end, a tailored RAKI model was evaluated in a first step. Compared to the original RAKI model, it achieved significantly lower NMSE compared to the original RAKI model on test data from the fastMRI neuro database for less than 30 ACS lines. However, the performance of tailored RAKI significantly declines when the number of ACS lines is further decreased. An iterative training approach is proposed that relies on an initial GRAPPA reconstruction for training data augmentation and iterative refining of the CNN weights using original and augmented ACS. To evaluate its robustness, iRAKI was tested on 200 different datasets assembled from the fastMRI neuro database. Using only 18 and 22 ACS lines for $R = 4$ and $R = 5$, respectively, it yields systematically enhanced NMSE and SSIM for different contrast settings in comparison to GRAPPA and standard RAKI. On a visual scale, iRAKI suppresses residual artifacts apparent in standard RAKI, whereas showing less noise-enhancement than GRAPPA. Therefore, iRAKI incorporates beneficial features from both methods.

The improved performance of iRAKI can be attributed to several aspects. First, the augmented ACS data allows for the use of a larger convolution filter size and helps to better capture the extended k-space "footprint" of the coil sensitivities.[9,10,22] Second, the augmented ACS data gain in accuracy after each reconstruction step. Analogous to SPIRiT,[31] both original and reconstructed data are used during k-space interpolation. After each iteration, the reconstructed samples become more accurate after applying the reconstruction kernel and re-inserting the original measured data. We emphasize that in iRAKI the original ACS lines are re-inserted after each iteration step, and the augmented ACS provide additional information. In contrast to SPIRiT, the convolution weights are refined after

each iteration in iRAKI. Decreasing the initial learning rate after each iteration ensures further robustness.

GRAPPA has been chosen as initial reconstruction, because it has proven to be robust with only few ACS lines and has only few reconstruction parameters. In this work, the number of central lines N from the initial GRAPPA reconstruction for training data augmentation was chosen empirically. In general, N should be chosen sufficiently large to benefit from the increased filter size assigned to the first hidden layer in tailored RAKI. However, we observed that the initial RAKI reconstruction appears noisier the larger N is chosen. The exact reason for this behavior is not yet clear. This may be because of an increased noise contamination as the amount of the GRAPPA-reconstructed training data increases compared to the amount of original training data. Alternatively, RAKI could exhibit a similar paradoxical behavior as GRAPPA regarding the impact of the amount and SNR of training data on the image quality. Therefore, further research is required to automatically determine an optimized amount of augmented ACS lines.

The scope of this work was to improve RAKI by iterative training. Another approach for improving RAKI includes residual RAKI[6] (rRAKI) that trains non-linear CNNs jointly with a linear convolution implemented via a skip connection. In our experience, however, rRAKI suffers from similar limitations regarding the amount of training data. Exemplary reconstructions with varying number of ACS lines are presented in Supporting Material S9. Similar to original RAKI, rRAKI performs well with more than 40 ACS lines at $R = 4$. However, for typical matrix size of 320×320 (e.g., often used in the fastMRI database), the effective acceleration factor increases from 2.9 to 3.4 when the number of ACS lines is reduced from 40 to 18.

Although GRAPPA can further be improved by iterative training, its performance is limited by the linearity. As shown in Figure S8, iRAKI outperformed iterative-GRAPPA for a wide range of imaging scenarios.

iRAKI relies on an initial GRAPPA reconstruction for training data augmentation. It is worth noting that this approach has also been proposed, but not demonstrated in the original RAKI article.[4] An initial parallel imaging reconstruction is also used in scan-specific artifact reduction in k-space (SPARK),[33] where a CNN is used to correct for k-space artifacts of the initial reconstruction to achieve better reconstruction quality. Future investigations may focus on the evaluation of an initial iRAKI reconstruction in SPARK to further enhance reconstruction quality.

Another approach based on an initial fast reconstruction is inspired by low-rank matrix modeling of local k-space neighborhoods (LORAKS)[34] and RAKI, and is termed LORAKI.[35] LORAKI translates the linear auto-calibrated-LORAKS method into a nonlinear deep learning method. LORAKI admits a wide range of sampling patterns, and even calibrationless patterns are possible if synthetic ACS data is generated with a fast initial reconstruction. However, it requires tuning of multiple parameters (e.g., rank, kernel sizes, and regularization parameters) and needs VCCs to capture the LORAKS phase constraints. In contrast, iRAKI is more flexible in terms of phase-constraints, and the use of VCCs is optional. It is worth noting that k-space inconsistencies such as non-periodic flow or motion may prevent the use of phase-constraints.

Additional flexibility of iRAKI stands in the varying contrast information between calibration- and undersampled data, because it prevents contrast contamination in standard RAKI (also shown in Dawood et al.[36]), while preserving its noise-resilience. In this work, it was demonstrated that iRAKI provides better image quality than GRAPPA and standard RAKI for the case of pre-scan calibration, which is often used in parallel imaging.

4.1 | Limitations and outlook

The performance of iRAKI was evaluated for standard 2D imaging so far. Its applicability for 3D imaging,[37,38] wave-encoding,[39] or simultaneous multi-contrast reconstruction (JVC-GRAPPA)[40] needs to be investigated in future works.

One drawback of iRAKI is the increased reconstruction time. The total training time in iRAKI amounts to $\approx$ 180 s and $\approx$ 170 s for $R = 4$ and $R = 5$, respectively, exceeding standard RAKI ($\approx$12 s and $\approx$20 s) and GRAPPA (<15 s both $R = 4$ and $R = 5$). Future work should focus on optimizing the training speed to apply iRAKI in clinical applications.

The performance of iRAKI is expected to depend on the reconstruction quality of the initial GRAPPA reconstruction. A general acceleration factor limit for the application of iRAKI cannot be specified, because the quality of the initial GRAPPA reconstruction depends on the base signal-to-noise ratio and the g-factor.[2,41] In our experience, iRAKI yields better image quality than GRAPPA and standard RAKI at $R = 6$, but the reconstructed images may not be of diagnostic value because of residual artifacts and noise enhancement (Figure S9). However, one should keep in mind that the acquisition of many ACS lines comes along with decreases overall acceleration. Depending on the matrix size of the final image, it may be faster to scan with fourfold undersampling and 18 ACS lines instead of sixfold undersampling and 48 ACS lines.

In this work, it was also investigated whether iRAKI yields comparable results to the image-based variational networks. The variational network showed better

denoising performance in comparison to iRAKI, when it is trained on a database, whose anatomy and contrast information matches to the target undersampled image. However, as shown in this work, VarNets may suffer from residual artifacts when this condition is not fulfilled, in accordance to previous findings.[42] In case of the development of novel MR sequences or the examination of uncommon anatomies, there may be a lack of large databases for end-to-end network training. For these situations, scan-specific iRAKI may be beneficial because it does not require large databases.

5 | CONCLUSION

The number and contrast of training samples are essential for standard RAKI reconstruction quality. Given a limited training data amount, the proposed iRAKI combines beneficial features of GRAPPA and standard RAKI and yields reconstructions with suppression of both noise and residual artifacts for standard 2D imaging. It shows flexibility in terms of different calibration approaches (pre-scan or integrated ACS) and implementation of phase-constrained reconstruction.

ACKNOWLEDGMENTS

The authors thank the anonymous referees for improving the manuscript, Moritz Blumenthal for implementing variational networks in BART and Dr. Fabian T. Gutjahr for constructive criticism of the manuscript. We thank dataSphere@JMU for providing informative discussions and the German Federal Ministry of Education and Research (BMBF) for funding project line VIP+ (03VP04951) and furthermore the Bavarian Ministry of Economic Affairs, Infrastructure, Transport and Technology. Open Access funding enabled and organized by Projekt DEAL. Open Access funding enabled and organized by Projekt DEAL.

FUNDING INFORMATION

German Federal Ministry of Education and Research (BMBF): 03VP04951; Bavarian Ministry of Economic Affairs, Infrastructure, Transport and Technology.

DATA AVAILABILITY STATEMENT

In the spirit of reproducible research, code the generate iRAKI, tailored RAKI and GRAPPA reconstructions shown in this work for in-line calibration and pre-scan setting with sample datasets is available under https://github.com/pdawood/iterativeRaki.

ORCID

Peter Dawood https://orcid.org/0000-0001-7127-607X

REFERENCES

1. Roemer PB, Edelstein WA, Hayes CE, Souza SP, Mueller OM. The NMR phased array. *Magn Reson Med*. 1990;16:192-225.
2. Pruessmann KP, Weiger M, Scheidegger MB, Boesiger P. SENSE: sensitivity encoding for fast MRI. *Magn Reson Med*. 1999;42:952-962.
3. Griswold MA, Jakob PM, Heidemann RM, et al. Generalized autocalibrating partially parallel acquisitions (GRAPPA). *Magn Reson Med*. 2002;47:1202-1210.
4. Akçakaya M, Moeller S, Weingärtner S, Uğurbil K. Scan-specific robust artificial-neural-networks for k-space interpolation (RAKI) reconstruction: database-free deep learning for fast imaging. *Magn Reson Med*. 2019;81:439-453.
5. Zhang C, Hosseini SAH, Weingärtner S, Ugurbil K, Moeller S, Akçakaya M. Optimized fast GPU implementation of robust artificial-neural-networks for k-space interpolation (RAKI) reconstruction. *PLoS ONE*. 2019;14:e0223315.
6. Zhang C, Moeller S, Demire OB, Ugurbil K, Akcakaya M. Residual RAKI: a hybrid linear and non-linear approach for scan-specific k-space deep learning. *Neuroimage*. 2022;256:119248.
7. Taylor L, Nitschke G. Improving deep learning with generic data augmentation. *Proceedings of the 2018 IEEE Symposium Series on Computational Intelligence (SSCI)*; 2018:1542-1547.
8. Shorten C, Khoshgoftaar TM. A survey on image data augmentation for deep learning. *Journal of Big Data*. 2019;6:60.
9. Jakob PM, Griswold MA, Edelman RR, Sodickson DK. AUTO-SMASH: a selfcalibrating technique for SMASH imaging. *SiMultaneous Acquisition of Spatial Harmonics MAGMA*. 1998;7:42-54.
10. Heidemann RM, Griswold MA, Haase A, Jakob PM. VD-AUTO-SMASH imaging. *Magn Reson Med*. 2001;45:1066-1074.
11. Lustig M, Donoho D, Pauly JM. Sparse MRI: the application of compressed sensing for rapid MR imaging. *Magn Reson Med*. 2007;58:1182-1195.
12. Knoll F, Hammernik K, Zhang C, et al. Deep-learning methods for parallel magnetic resonance imaging reconstruction: a survey of the current approaches, trends, and issues. *IEEE Signal Processing Magazine*. 2020;37:128-140.
13. Dawood P, Blaimer M, Breuer F, Jakob PM, Oberberger J, et al. Iterative RAKI with complex-valued convolution for improved image reconstruction with limited training samples. *Proceedings of the 30th Annual Meeting of ISMRM*; 2022 Abstract Program Number 1193.
14. Virtue P. *Complex-Valued Deep Learning with Applications to Magnetic Resonance Image Synthesis*. Doctoral Dissertation. University of California at Berkeley; 2019.
15. Cole E, Cheng J, Pauly J, Vasanawala S. Analysis of deep complex-valued convolutional neural networks for MRI reconstruction and phase-focused applications. *Magn Reson Med*. 2021;86:1093-1109.
16. Trabelsi C, Bilaniuk O, Zhang Y, et al. Deep Complex Networks. *Proceedings of the 6th International Conference on Learning Representations, (ICLR 2018), Conference Track Proceedings*; 2018.
17. Nair V, Hinton GE. Rectified linear units improve restricted Boltzmann machines. *Proceedings of the 27th International Conference on International Conference on Machine Learning ICML'10*; 2010:807-814.

18. LeCun Y, Bengio Y, Hinton G. Deep learning. *Nature*. 2015;521:436-444.
19. Kingma DP, Ba J. Adam: a method for stochastic optimization. *Proceedings of 3rd International Conference on Learning Representations*. ICLR; 2015.
20. Paszke A, Gross S, Massa F, et al. PyTorch: an imperative style, high-performance deep learning library. *Proceedings of the 33rd Conference on Neural Information Processing Systems*; 2019.
21. Knoll F, Murrell T, Sriram A, et al. Advancing machine learning for MR image reconstruction with an open competition: overview of the 2019 fastMRI challenge. *Magn Reson Med*. 2020;84:3054-3070.
22. Bauer S, Markl M, Honal M, Jung BA. The effect of reconstruction and acquisition parameters for GRAPPA-based parallel imaging on the image quality. *Magn Reson Med*. 2011;66:402-409.
23. Sandino CM, Lai P, Vasanawala SS, Cheng JY. Accelerating cardiac cine MRI using a deep learning-based ESPIRiT reconstruction. *Magn Reson Med*. 2021;85:152-167.
24. Nencka AS, Arpinar VE, Bhave S, et al. Split-slice training and hyperparameter tuning of RAKI networks for simultaneous multi-slice reconstruction. *Magn Reson Med*. 2021;85:3272-3280.
25. Zhao T, Hu X. Iterative GRAPPA (iGRAPPA) for improved parallel imaging reconstruction. *Magn Reson Med*. 2008;59:903-907.
26. Wang Z, Bovik AC, Sheikh HR, Simoncelli EP. Image quality assessment: from error visibility to structural similarity. *IEEE Trans Image Process*. 2004;13:600-612.
27. Uecker M, Lai P, Murphy MJ, et al. ESPIRiT—an eigenvalue approach to autocalibrating parallel MRI: where SENSE meets GRAPPA. *Magn Reson Med*. 2014;71:990-1001.
28. Blaimer M, Gutberlet M, Kellman P, Breuer F, Koestler H, Griswold M. Virtual coil concept for improved parallel MRI employing conjugate symmetric signals. *Magn Reson Med*. 2009;61:93-102.
29. Hammernik K, Klatzer T, Kobler E, Pock T, Knoll F, et al. Learning a variational network for reconstruction of accelerated MRI data. *Magn Reson Med*. 2018;79:3055-3071.
30. Uecker M, Ong F, Tamir JI, Bahri D, Virtue P, et al. Berkeley advanced reconstruction toolbox. *Proceedings of the 23th Annual Meeting of ISMRM*. Vol 23; 2015:2486.
31. Lustig M, Pauly JM. SPIRiT: iterative self-consistent parallel imaging reconstruction from arbitrary k-space. *Magn Reson Med*. 2010;64:457-471.
32. Ding Y, Xue H, Ahmad R, Chang T-c, Ting ST, Simonetti OP. Paradoxical effect of the signal-to-noise ratio of GRAPPA calibration lines: a quantitative study. *Magn Reson Med*. 2015;74:231-239.
33. Arefeen Y, Beker O, Cho J, Yu H, Adalsteinsson E, Bilgic B. Scan-specific artifact reduction in k-space (SPARK) neural networks synergize with physics-based reconstruction to accelerate MRI. *Magn Reson Med*. 2022;87:764-780.
34. Haldar JP. Low-rank modeling of local k-space neighborhoods (LORAKS) for constrained MRI. *IEEE Trans Med Imaging*. 2014;33:668-681.
35. Kim TH, Garg P, Haldar JP. LORAKI: Reconstruction of undersampled k-space data using scan-specific autocalibrated recurrent neural networks. *Proceedings of the 27th Annual Meeting of ISMRM*; 2019 Abstract Program Number 4647.
36. Dawood P, Blaimer M, Jakob PM, Oberberger J. Influence of training data on RAKI reconstruction quality in standard 2D imaging. *Proceedings of the 29th Annual Meeting of ISMRM*, (Virtual Meeting); 2021 Abstract Program Number 1961.
37. Weiger M, Pruessman KP, Boesiger P. 2D SENSE for faster 3D MRI. *MAGMA*. 2002;14:10-19.
38. Breuer FA, Blaimer M, Mueller MF, et al. Controlled aliasing in volumetric parallel imaging (2D CAIPIRINHA). *Magn Reson Med*. 2006;55:549-556.
39. Bilgic B, Gagoski BA, Cauley SF, Fan CA, Polimeni JR, et al. Wave-CAIPI for highly accelerated 3D imaging. *Magn Reson Med*. 2015;73:2152-2162.
40. Bilgic B, Kim TH, Liao C, et al. Improving parallel imaging by jointly reconstructing multi-contrast data. *Magn Reson Med*. 2018;80:619-632.
41. Breuer F, Kannengiesser S, Blaimer M, Seiberlich N, Jakob P, Griswold M. General formulation for quantitative G-factor calculation in GRAPPA reconstructions. *Magn Reson Med*. 2009;62:739-746.
42. Hammernik K, Schlemper J, Qin C, Duan J, Summers RM, Rueckert D. Systematic evaluation of iterative deep neural networks for fast parallel MRI reconstruction with sensitivity-weighted coil combination. *Magn Reson Med*. 2021;86:1859-1872.

SUPPORTING INFORMATION

Additional supporting information may be found in the online version of the article at the publisher's website.

Figure S1 (A) Architecture of the tailored convolutional neural network (CNN) used for RAKI implementation in this work. Convolution is performed with complex-valued filter matrices. The input-layer takes in the zero filled, k-space data, therefore, having N_c channels, with N_c denoting the number of receiver coils. The first and second hidden layers are assigned 256 and 128 channels, respectively. The output layer predicts all missing k-space data across all coils, therefore, having $(R-1)\times N_c$ channels, with R denoting the undersampling rate. (B) Boxplots of the normalized mean-squared-error (NMSE, top) and the structural similarity index measure (SSIM, bottom) for GRAPPA, original RAKI and tailored RAKI evaluated on cohorts from the fastMRI neuro database (50 datasets for each T_1, T_1post, T_2, and FLAIR). (C) GRAPPA, original RAKI and tailored RAKI in comparison shown for exemplary sampled datasets of evaluated fastMRI cohorts from B. Error maps are shown below, and include NMSE, PSNR, and SSIM (from top to bottom).

Figure S2 GRAPPA, standard RAKI and iRAKI evaluated on the T_1-neuro2 dataset at four- and fivefold retrospectively undersampling ($R = 4$, left column and $R = 5$, right column) using 18 and 22 ACS lines as training data, respectively. Error maps are shown below, and include NMSE, PSNR, and SSIM. Reconstructions were performed without phase constrains (top row) and including the virtual-conjugate-coils (VCC) concept (bottom row).

Figure S3 GRAPPA, standard RAKI and iRAKI evaluated on the T_2-neuro2 dataset at four- and fivefold retrospectively undersampling ($R = 4$, left column and $R = 5$, right column) using 18 and 22 ACS lines as training data, respectively. Error maps are shown below, and include NMSE, PSNR, and SSIM. Reconstructions were performed without phase constrains (top row) and including the virtual-conjugate-coils (VCC) concept (bottom row).

Figure S4 GRAPPA, standard RAKI and iRAKI evaluated on the T_1-neuro1 dataset at four- and fivefold retrospectively undersampling ($R = 4$, left column and $R = 5$, right column) using 18 and 22 ACS lines as training data, respectively. Error maps are shown below, and include NMSE, PSNR, and SSIM. Reconstructions were performed without phase constrains (top row) and including the virtual-conjugate-coils (VCC) concept (bottom row).

Figure S5 GRAPPA, standard RAKI and iRAKI evaluated on the T_1-neuro3 dataset at four- and fivefold retrospectively undersampling ($R = 4$, left column and $R = 5$, right column) using 18 and 22 ACS lines as training data, respectively. Error maps are shown below, and include NMSE, PSNR, and SSIM. Reconstructions were performed without phase constrains (top row) and including the virtual-conjugate-coils (VCC) concept (bottom row).

Figure S6 GRAPPA, standard RAKI and iRAKI evaluated on the T_2-neuro3 dataset at four- and fivefold retrospectively undersampling ($R = 4$, left column and $R = 5$, right column) using 18 and 22 ACS lines as training data, respectively. Error maps are shown below, and include NMSE, PSNR, and SSIM. Reconstructions were performed without phase constrains (top row) and including the virtual-conjugate-coils (VCC) concept (bottom row).

Figure S7 iRAKI and the variational network (VarNet) in comparison for scans with T_1-, T_1post-, T_2-, and FLAIR-weighting (from left to right and top to bottom). The VarNet was trained one knee-data with proton-density weighting. Error maps are shown at the bottom and include NMSE, PSNR, and SSIM w.r.t. the fully sampled reference image.

Figure S8 (A) Boxplots of NMSE (top) and SSIM (bottom) for GRAPPA, iterative-GRAPPA, standard RAKI, and iRAKI evaluated on cohorts assembled form the fastMRI neuro-database. Four different contrast were considered (T_1, T_1post, T_2, and FLAIR), and 50 datasets per contrast were retrospectively undersampled at rate 4 (left) and rate 5 (right) using 18 and 22 ACS lines, respectively.(B) Exemplary image reconstructions from evaluations depicted in A (left: T_1post fourfold undersampling, right: FLAIR fivefold undersampling). Error maps are shown at the bottom and include NMSE, PSNR and SSIM w.r.t. the fully sampled reference image. (C) T_1-neuro2-dataset (left, fourfold undersampling, 18 ACS lines) and T_1-neuro1-dataset (right, fivefold undersampling, 22 ACS lines) reconstructed with GRAPPA, iterative-GRAPPA, standard RAKI, and iRAKI including the VCC concept.

Figure S9 GRAPPA, standard RAKI and iRAKI evaluated on sixfold retrospectively undersampling of T_1-neuro1-dataset. Twenty-eight ACS lines were used as training data (re-inserted into reconstructed k-spaces). Error maps are shown below, and include NMSE, PSNR, and SSIM difference metrics.

Supporting Material S1 mp4-Movie image reconstructions of GRAPPA, standard RAKI and iRAKI evaluated on varying training data amount (Figure 2). Error maps are shown below, and include NMSE, PSNR, and SSIM difference metrics w.r.t. the fully sampled reference image.

Supporting Material S2 mp4-Movie image reconstructions of VarNet, rRAKI, and iRAKI evaluated on varying training data amount. Error maps are shown below, and include NMSE, PSNR and SSIM difference metrics w.r.t. the fully sampled reference image.

How to cite this article: Dawood P, Breuer F, Stebani J, et al. Iterative training of robust k-space interpolation networks for improved image reconstruction with limited scan specific training samples. *Magn Reson Med*. 2023;89:812-827. doi: 10.1002/mrm.29482